Measuring surface energy of solid surfaces using centrifugal adhesion balance

Appu Vinod,[1] Yuval Barak,[1] Sakshi Yadav Schmid,[2,3] Semih Gulec,[4] Yagnavalkya Bhimavarapu,[4] Akash Jena,[4] David Katoshevski,[1] Nitsa Haikin,[5] and Rafael Tadmor[1,*]

[1]*Department of Mechanical Engineering, Ben Gurion University, Beer-Sheva 84105, Israel*
[2]*Materials Transformation, Pacific Northwest National Laboratory, Richmond, Washington 99352, USA*
[3]*Material Science and Engineering, University of Washington, Seattle, Washington 98195-2120, USA*
[4]*Dan F. Smith Department of Chemical Engineering, Lamar University, Beaumont, Texas 77705, USA*
[5]*Department of Physics, NRCN, Beer Sheva 84150, Israel*

(Received 12 December 2023; accepted 17 April 2024; published 3 July 2024)

The standard way to evaluate the solid surface energy using probe liquids relies on contact angle measurements. The measured contact angles rely on visible means and are different from their nanoscopic thermodynamic values. This compromises the surface-energy predictions so much that the surface energy-values can be hundreds of percentages higher than expected based on comparisons with different methods as reported in several studies. We consider the Owen-Wendt approach, which breaks the surface energy to polar and dispersive components, and present a technique for measuring surface energy of solids using probe liquids. Our method avoids the need to measure contact angles; instead, it uses solid-liquid work of adhesion measurements which are performed using a centrifugal adhesion balance. In agreement with the studies mentioned above, we found that indeed, the surface energies of the measured solids are significantly lower than those based on contact angle measurements. More importantly we found that our method results in a reasonable breakdown of the surface energy to polar and dispersive components with a higher polar component for more polar solids. This is in contrast with the surface energy based on contact angle measurements for which the breakdown did not make sense, i.e., the measurements reflected higher polar components of the surface energy for less polar solids.

DOI: 10.1103/PhysRevE.110.014801

I. INTRODUCTION

Unlike surface energy of a liquid, the surface energy of a solid cannot be directly measured. Instead, the contact angles from a set of probe liquids on a given solid are used for the determination of the liquids' work of adhesion to the solid through the Young-Dupre equation [1]. These solid-liquid works of adhesion values are then used in several mathematical models [2–4] to determine the solid surface energy [5–8]. One problem with all these models is that they use visible contact angle measurements to estimate the solid-liquid work of adhesion values. The visible contact angle values are different from the true, nanoscopic, contact angles that we need for the surface-energy calculations. Indeed, people used other methods to study the solid-liquid work of adhesion. Some of them used techniques such as atomic force microscopy (AFM) [9,10], AFM with PeakForce quantitative nanomechanical mapping [11], and scanning force microscope (SFM) [12], which require significant time investment, and provide indirect measurements of the work of adhesion. Others [13–15], as well as the study reported here, use the centrifugal adhesion balance (CAB), which provides direct measurements and can take several minutes. All these studies show that the reliance on visible contact angles to obtain the work of adhesion through the Young-Dupre equation (i) overestimates solid-liquid work of adhesion measurements typically by hundreds of percentages [9–14], and (ii) fails to provide suitable qualitative predictions [9–14]. The reason contact angles overestimate the solid liquid work of adhesion has been attributed [14,16] to minute deformations (adaptations) [17] that are highest at the triple line (from which it also starts) [16,18–20]. To address the true surface energy, Bormashenko *et al.* showed that the work of adhesion of a drop depended on the wetting properties of the entire area on which it rested [21]. Chen and Nosonovsky [22] provide a limit for the lowest surface energy that one can expect. Yet, an exact determination of the surface energy of solids is still lacking. The motivation to obtain an accurate method for measurements of surface energy comes from the need to evaluate the tendency of airborne particulates to stick to each other or adsorb other elements, which grows with their surface energy.

In this paper, we describe a method to evaluate the surface-energy values of solids where, instead of contact angles, it relies on direct work of adhesion measurement. We consider the Owen-Wendt theory [4] and modify it for our approach; then, we examine the results and compare them with those obtained from contact angle measurements. We see that the results obtained from work of adhesion values are more reasonable than those obtained by using contact angles. Specifically, the results obtained with contact angles resulted in surface-energy values that were significantly higher than expected, while when relying on the work of adhesion, such concerns were not observed.

*Corresponding author: tadmorr@bgu.ac.il

II. THEORY

A. Selecting the criterion for determination of the surface energy

As mentioned in the Introduction, the solid-air surface energy has traditionally been estimated based on measurements of visible contact angles [23,24]. These values were then plugged into one of several mathematical models to determine the surface energy of the solid. There are several contact angles that can be considered:

(i) The as-placed contact angle. This is best obtained by carefully placing the drop so that no inertia is added to the drop when it is placed [25]. The rationale of using this contact angle stems from the fact that it is the most commonly used contact angle for such calculations [26,27].

(ii) Advancing contact angle obtained by inflating the drop. The contact angle is measured at the point the drop triple line depins. The rationale of using the advancing contact angle stems from the knowledge [9,10,13,14,28,29] that the true work of adhesion is lower than the value obtained when considering the as-placed contact angle in the Young-Dupre equation. To get a lower work of adhesion we need to have higher contact angles, namely advancing contact angles.

(iii) Receding contact angle obtained by deflating the drop. The contact angle is measured at the point the drop triple line depins. The rationale of using the receding contact angle is related to experiments in which drops are made to fly off the surface in the normal direction. In such experiments, as the drop is pulled and detached from the surface, it obtains a bell shape temporarily and its contact angle decreases, namely gets closer to the receding value.

(iv) The weighted average contact angle, θ_o, calculated from the advancing and receding contact angles [30]:

$$\theta_o = \cos^{-1}\left(\frac{\Gamma_A \cos\theta_A + \Gamma_R \cos\theta_R}{\Gamma_A + \Gamma_R}\right), \tag{1}$$

where

$$\Gamma_A = \left(\frac{\sin^3\theta_A}{(2-3\cos\theta_A + \cos^3\theta_A)}\right)^{(1/3)} \tag{2}$$

and

$$\Gamma_R = \left(\frac{\sin^3\theta_R}{(2-3\cos\theta_R + \cos^3\theta_R)}\right)^{(1/3)}. \tag{3}$$

The rationale of using this contact angle stems from the fact that in the case where the energy cost associated with the advancing contact angle equals that of the receding contact angle; θ_o, is (under certain assumptions [30]) the equilibrium thermodynamic contact angle [31–34].

The contact angles mentioned above provide estimates for the work of adhesion. As we shall see, all these options will result in work of adhesion values that overestimate the one measured using the CAB. Considering literature studies [9,10,14], these are overestimates of the true of work of adhesion values, and, therefore, also overestimate the surface energy of the solid.

(v) The work of adhesion measured using the CAB [14,28,29,35,36]. The rationale of using this option stems from the fact that CAB measurements are considered to provide the true work of adhesion values [37,38].

In this paper, we chose to compare the five options above using the mathematical model by Owen-Wendt [4]. For options (i)–(iv), the Owen-Wendt model is used in the conventional way, and for the fifth option, we modify it for CAB measurements so that it directly considers the solid-liquid work of adhesion.

B. Modifying the Owen-Wendt theory for CAB measurements

The Owen-Wendt theory aims to calculate the surface energy of a solid by considering it as the sum of the energy contributions from the intermolecular interactions that give rise to the interface. They considered particularly dispersive and polar interactions. Thus, their surface energy, γ_{12}, is described by Eq. (4),

$$\gamma_{12} = \gamma_{12}^d + \gamma_{12}^p, \tag{4}$$

where the subscript 1 can be solid, liquid, or vapor (subscripts S, L, or V) and the same for subscript 2, and the superscripts d and p refer to the dispersive and the polar components.

The Owen-Wendt model is based on the Fowkes model [39] that was the first to suggest that the interfacial energy, γ_{12}, of an interface that has only dispersive interactions can be described by Eq. (5):

$$\gamma_{12} = \gamma_1 + \gamma_2 - 2\sqrt{\gamma_1^d \gamma_2^d}. \tag{5}$$

Note that the dispersive interaction is only between phase 1 and phase 2. Phase 1 itself may have other interactions and so does phase 2, but the only interaction that is common to both liquids is the dispersive interaction, and therefore this is the only interaction that causes a reduction in the interfacial energy between the two phases. For example, for hexadecane (*HD*) and water, Eq. (5) would look like Eq. (6):

$$\gamma_{HD\text{-water}} = \gamma_{HD} + \gamma_{\text{water}} - 2\sqrt{\gamma_{HD}^d \gamma_{\text{water}}^d}. \tag{6}$$

Since $\gamma_{HD} = \gamma_{HD}^d$, Eq. (6) has only one unknown and can be solved for γ_{water}^d.

In Eq. (7), we rewrite Eq. (5) for the case of a solid and liquid:

$$\gamma_{\text{SL}} = \gamma_{\text{SV}} + \gamma_{\text{LV}} - 2\sqrt{\gamma_{\text{SV}}^d \gamma_{\text{LV}}^d}. \tag{7}$$

To solve Eq. (7), Fowkes considered the Young equation [Eq. (8)]:

$$\gamma_{\text{SV}} = \gamma_{\text{SL}} + \gamma_{LV}\cos\theta, \tag{8}$$

and from Eq. (8) and Eq. (7) we get Eq. (9),

$$\cos\theta = -1 + 2\sqrt{\gamma_{\text{SV}}^d}\left(\frac{\sqrt{\gamma_{\text{LV}}^d}}{\gamma_{\text{LV}}}\right). \tag{9}$$

Equation (9) can be solved using data for the dispersive components of the liquid's surface tension, γ_{LV}^d . To get γ_{LV}^d , Fowkes used liquids that had only dispersive interactions (specifically hydrocarbons) and measured their interfacial tensions with another liquid whose surface tension was known

TABLE I. Liquid-vapor surface tension of the four probe liquids used in this study.

Probe liquids	Polar components of the interfacial tension (γ_{LV}^{p})	Dispersive components of the interfacial tension (γ_{LV}^{d})	Liquid-vapor interfacial tension ($\gamma_{LV} = \gamma_{LV}^{p} + \gamma_{LV}^{d}$)
Water	51.0	21.8	72.8
Glycerol	30.0	34.0	64.0
Ethylene glycol	19.0	29.0	48.0
Diiodomethane	2.30	48.5	50.8

(e.g., water). Then, he used Eq. (6) to solve for the dispersive components of the surface tension of the water or other liquids.

From Eq. (9), Fowkes calculated γ_{SV}^{d} by creating a plot of $\cos\theta$ vs $(\frac{\sqrt{\gamma_{LV}^{d}}}{\gamma_{LV}})$. Theoretically, it should form a straight line with a slope of $2\sqrt{\gamma_{SV}^{d}}$. Since the interception with the y axis is always fixed (-1), just one measurement of the contact angle (θ) is enough to figure out the dispersion force component of the solid (γ_{SV}^{d}) if the measurement is done using a liquid whose dispersive surface energy is known [cf. Eq. (6)].

Later, Owen and Wendt provided a more generalized form for Eq. (5) by including the contributions from the polar components as well [Eq. (10)]:

$$\gamma_{SL} = \gamma_{SV} + \gamma_{LV} - 2\sqrt{\gamma_{SV}^{d}}\sqrt{\gamma_{LV}^{d}} - 2\sqrt{\gamma_{SV}^{p}}\sqrt{\gamma_{LV}^{p}}. \quad (10)$$

Thus, based on Eq. (10), Eq. (9) can be given in a more generalized form as

$$\frac{\gamma_{LV}(1+\cos\theta)}{2\sqrt{\gamma_{LV}^{d}}} = \sqrt{\gamma_{SV}^{d}} + \sqrt{\gamma_{SV}^{p}}\left(\sqrt{\frac{\gamma_{LV}^{p}}{\gamma_{LV}^{d}}}\right), \quad (11)$$

where, in the linear equation $y = ax + b$, $y = \frac{\gamma_{LV}(1+\cos\theta)}{2\sqrt{\gamma_{LV}^{d}}}$, $a = \sqrt{\gamma_{SV}^{p}}$, $x = \sqrt{\frac{\gamma_{LV}^{p}}{\gamma_{LV}^{d}}}$, and $b = \sqrt{\gamma_{SV}^{d}}$.

Generally, a plot of $(\frac{\gamma_{LV}(1+\cos\theta)}{2\sqrt{\gamma_{LV}^{d}}})$ vs $(\sqrt{\frac{\gamma_{LV}^{p}}{\gamma_{LV}^{d}}})$ for different probe liquids should give a straight line with a slope that equals $\sqrt{\gamma_{SV}^{p}}$ and an intercept with the y axis that equals $\sqrt{\gamma_{SV}^{d}}$ [40]. The intercept represents the square root of the dispersive component, and the slope represents the square root of the polar component of the solid surface energy. Finally, the solid surface energy is obtained by adding the squares of the slope and the intercept to obtain Eq. (4).

Note that both Fowkes and Owen-Wendt models do not consider work of adhesion, yet the equations of both models include the expression $\gamma_{LV}(1+\cos\theta_Y)$, which happened to represent the work of adhesion, W_{SL}, according to the Young-Dupre equation [Eq. (12)]:

$$W_{SL} = \gamma_{LV}(1+\cos\theta_Y), \quad (12)$$

where θ_Y is the Young equilibrium contact angle. However, the measured macroscopic contact angle differs from the Young one, which is nanoscopic [16]. It can be advancing, receding, as placed, or anything in between. As we shall see, all these contact angles result in overestimated work of adhesion values. We write Eq. (13) for these, contact angle-based (and overestimated) works of adhesion values:

$$W_{SL,\,CA} = \gamma_{LV}(1+\cos\theta_{apparent}), \quad (13)$$

where $W_{SL,\,CA}$ represents the work of adhesion values calculated using the different contact angles mentioned earlier, which is represented by $\theta_{apparent}$.

In our case, since we can measure the work of adhesion directly, we replace $\gamma_{LV}(1+\cos\theta)$ in Eq. (11) with the CAB measured work of adhesion, $W_{SL,\,CAB}$. In this case, the work of adhesion is obtained from the force at which the three-phase contact line starts shrinking spontaneously, which we term here the pull-off force, F_D, and the corresponding diameter as D_p:

$$W_{SL} = \frac{F_D}{\pi D_p}, \quad (14)$$

where D_p is the diameter from which the drop starts shrinking spontaneously. Considering that the CAB may have its own experimental errors, we use the term $W_{SL,\,CAB}$ to represent the CAB measured work of adhesion.

Now, we rewrite Eq. (11) as Eq. (15) below:

$$\frac{W_{SL}}{2\sqrt{\gamma_{LV}^{d}}} = \sqrt{\gamma_{SV}^{p}}\sqrt{\frac{\gamma_{LV}^{p}}{\gamma_{LV}^{d}}} + \sqrt{\gamma_{SV}^{d}}. \quad (15)$$

A plot of $(\frac{W_{SL}}{2\sqrt{\gamma_{LV}^{d}}})$ vs $(\sqrt{\frac{\gamma_{LV}^{p}}{\gamma_{LV}^{d}}})$ for different probe liquids should give a straight line with an intercept of $\sqrt{\gamma_{SV}^{d}}$ and a slope of $\sqrt{\gamma_{SV}^{p}}$, from which we calculate the surface energy of the solid-vapor interface according to Eq. (4).

The Owen-Wendt method [4] considers probe liquids. These are liquids whose surface tensions are theoretically decomposed into two parts, polar and dispersive components, whose sum gives the surface tension of the liquid [41–43]. The most common probe liquids used in the Owen-Wendt method for the evaluation of the solid's surface energy are listed in Table I along with their liquid-vapor interfacial tensions [44,45].

C. Determination of the work of adhesion using CAB

The way to determine the solid-liquid work of adhesion via CAB measurements was discussed in the past [14]. Briefly, we increase the weight of a suspended drop at constant mass, by increasing the effective gravity pulling on it, and measure the reduction in the diameter of the drop. As mentioned earlier, at the pull-off force F_D, the drop diameter shrinks spontaneously, following which the whole drops either detaches from the

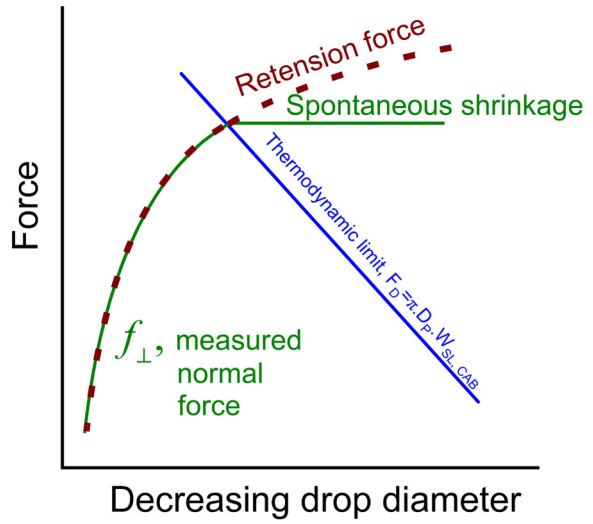

FIG. 1. A graph that shows the force pulling on a drop, $f_\perp$, vs. the drop's circumference as a negative abscissa. Once the force intersects with the thermodynamic limit, the circumference of the drop decreases spontaneously. This spontaneous reduction is represented by the green line. (Based on Tadmor *et al.* [14]).

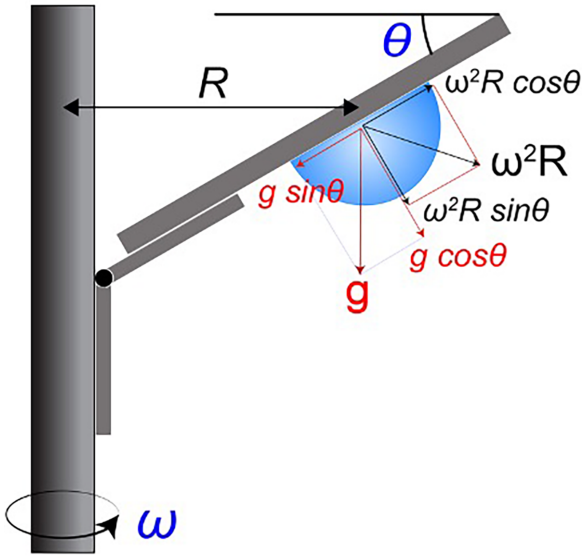

FIG. 3. Schematics describing the CAB alignment when the summation of the lateral forces is zero and the normal force is pulling on the drop. As the normal force increases, the drop gets elongated and eventually detaches from the surface.

solid or, if the necking is thin enough, the neck itself snaps. Provided this shrinkage is indeed spontaneous (namely can occur without an increase in the force), this detachment of the drop happens when the retention force reaches its thermodynamic limit as shown in Fig. 1.

Figure 2 shows pictures of a water drop that is subjected to a normal force (induced by the CAB) that pulls on the drop and eventually detaches it from the Octadecyl trimethoxy silane (OTMS)-coated silicon surface, while leaving a baby droplet behind. We see that as the force increases, the droplet elongates until the normal acceleration reaches –4.8 g (its thermodynamic limit, cf. F_D in Fig. 2) from which the drop's circumference reduces spontaneously.

The calculation of the work of adhesion is based on an analogy to Tate's law, i.e., using the critical diameter that corresponds to the point at which the drop starts shrinking spontaneously without the need to further increase the force. Note that the point of detachment in Fig. 2 corresponds to the fourth frame, not the fifth. The fifth represents the liquid-liquid snapping, which corresponds to the liquid-air surface tension, while the fourth corresponds to the spontaneous shrinkage of the triple line, which represents the work of adhesion. Both in Tate's surface tension case and in our work of adhesion case, the end of the process does not represent a thermodynamic property. In Tate's law, the end of the process is the detachment of the last two molecules, while the thermodynamic property is described by the spontaneous shrinkage of the liquid's neck. In our case, the end of the process is also described by the detachment of two molecules while the work of adhesion is described by the spontaneous shrinkage of the triple line. In both cases a spontaneous shrinkage event determines the thermodynamic property.

III. METHOD AND MATERIALS

In our study, the solid-liquid work of adhesion is measured by increasing the effective gravity pulling on a drop of constant mass so that it becomes heavier until it detaches from the solid-liquid interface. We then look for a critical force beyond which there is a spontaneous reduction in the drop's width (namely, the circumference will continue reducing even if the force is not increased). To increase the drop's weight the CAB combines gravitational and centrifugal forces such that their lateral components cancel each other but their normal components add up and are gradually increased while pointing to the same direction (normal pulling).

A schematic diagram of the CAB is shown in Fig. 3. Equations (16) and (17) describe the relation between the gravitational and the centrifugal forces and the resultant

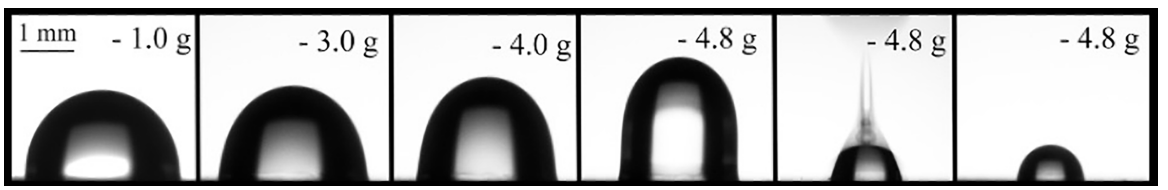

FIG. 2. Pictures of 8.0-μ*l* water drop on an OTMS-coated silicon surface, during a CAB run of an increasing normal force (effective gravity) which pulls on the drop, where *g* is the gravitational acceleration.

normal and lateral forces ($f_\perp$ and $f_\parallel$) acting on the drop:

$$f_\parallel = m(\omega^2 R\cos\alpha - g\sin\alpha), \tag{16}$$

$$f_\perp = m(\omega^2 R\sin\alpha + \cos\alpha), \tag{17}$$

where m is the drop's mass, ω is the CAB angular velocity, R is the drop's distance from the CAB's center of rotation, g is the gravitational acceleration, and α is the tilt angle with respect to the horizon. For the experiments done in this study, $f_\parallel = 0$ was maintained while $f_\perp$ was gradually increased.

In order to ensure that the droplet volume remains constant, we seal the drop with an optically transparent hemisphere. In addition, for longer experiments, we also place several droplets (satellite droplets, whose volume is smaller than the main droplet) around the main droplet so that the air in the hemisphere gets saturated quickly. The relative humidity inside this closed environment reaches roughly 96% within about 3 minutes [46], which suppresses the evaporation of the main droplet.

Other techniques for measuring forces between a drop and a solid surface use a force gauge that is attached to a solid object that, in one way or another, touches the drop such as the drop adhesion force instrument (DAFI) [47] or other methods [48,49]. The uniqueness of the CAB relates to two features: (1) No external object touches the drop. Instead, the measured forces are the body forces acting on the drop; and (2) It allows for decoupling between the gravitational and centrifugal forces allowing any combination between the lateral and normal body forces [14,28,29,35,36,50]. In the present study, as well as in studies by other authors [15], the lateral force is set to zero and the effective gravity is increased gradually (at a pace of that typically ranges from 0.01 μN–0.3 μN/s).

Materials

Surface energy was measured for four different surfaces.

The PTFE (polytetrafluoroethylene, a 1.6-mm-thick board (item No. 45446 bought from U.S. Plastic Corp.) was cleaned with ethanol (99.5%) obtained from Sigma-Aldrich and with deionized water (Barnstead Nanopure Purification specific conductance (25 °C)$\leqslant 0.7\times10^{-6}\Omega^{-1}\,\mathrm{cm}^{-1}$). The Teflon was then dried in vacuum at 100 °C for 15 min.

To obtain silanized surfaces, two different silanization processes were practiced on silicon wafers obtained from Virginia Semiconductor, VA (diameter: 76.2 ± 0.3 mm, orientation: ⟨110⟩ ± 0.9°, dopant: Boron, resistivity: 0.0034−0.0046Ω-cm, center thick- ness: 381 μm ± 25 μm). One silanization was with OTMS [51] (90% technical grade, CAS No. 3069–42–9) obtained from Sigma-Aldrich, and the other was with Phenyltrichlorosilane (PTCS) (97% technical grade, CAS No. 98–13–5) obtained from Sigma-Aldrich.

To silanize the silicon substrates using OTMS, we adopted the process described in earlier studies [52]. Briefly, in this process the silicon wafers are initially rinsed with deionized water, then with acetone, and then with deionized water again. Next, the wafers are dried in a StableTemp vacuum oven (model No. 5053–10 from Cole-Parmer) at 100 °C for 30 min. Subsequently, an ultraviolet-ozone surface treatment (UV/ozone model No. Procleaner 110) is carried out for 45 min. Following this, the wafers are immersed in 1 vol. % OTMS/Toluene solution at 95 °C for 3 hours. Finally, the silanized surface is rinsed with deionized water and dried in the vacuum for 45 min at 80 °C.

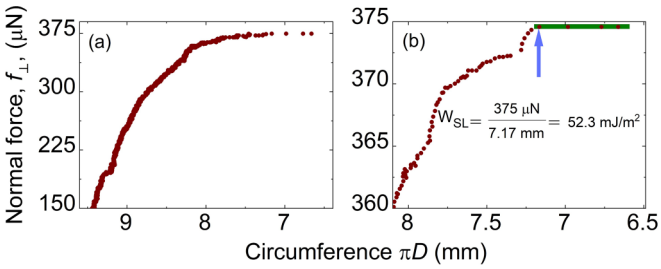

FIG. 4. (a) The circumference of the triple line of an 8.0-μl water drop on an OTMS-coated silicon surface vs the normal body force pulling on the drops. (b) Zoom-in on the end of the run presented in (a) where the blue arrow shows the values taken for the pull-off force and the pull-off diameter in Eq. (14). The green line corresponds to the green line in Fig. 1.

To silanize the silicon substrates using PTCS, we adopted a similar method which was used to silanize the surfaces using OTMS. First, the silicon wafers are rinsed with deionized water, then with acetone, and then with deionized water again. Next, the wafers are dried in a StableTemp vacuum oven (model No. 5053–10 from Cole-Parmer) at 100 °C for 30 min. Subsequently, an ultraviolet-ozone surface treatment (UV/ozone model No. Procleaner 110) is carried out for 45 min. Following this, the wafers are immersed in 1 vol. % PTCS/toluene solution at 120 °C for 1 hour. Finally, the silanized surface is rinsed with deionized water and dried in the vacuum over for 45 min at 80 °C.

Paraffin wax (Sigma-Aldrich, CAS No. 8002–74–2) was obtained in pellet form and melted in a Petri dish to obtain a flat surface. A rectangular piece of about 2 cm × 1 cm was cut from it and placed inside the sample holder of the CAB for the experimental run.

Four different probe liquids with known surface tension values were used to measure surface energy of the solids: (1) Deionized water; (2) Glycerol (Sigma-Aldrich, ⩾ 99.5% technical grade, CAS No. 56–81–5); (3) Ethylene glycol (anhydrous, Sigma-Aldrich, ⩾ 99.8% technical grade, CAS No. 107–21–1); and (4) Diiodomethane (MI) (MilliporeSigma, ⩾98% technical grade, CAS No. 75–11–6).

IV. RESULTS

We used four liquids to get the surface energy of one solid surface by linear regression. Figure 4 shows an example of an experimental run for the work of adhesion of water with OTMS.

Similarly, Fig. 5 shows an example of an experimental run for the work of adhesion of ethylene glycol drop to PTFE.

The work of adhesion (W_{SL}) values of the four probe liquids on the four different solid surfaces, obtained using CAB measurements, are shown in Table II. We see that the work of adhesion of water is higher for PTFE, OTMS, and PTCS, but is lower for paraffin wax.

To compare the work of adhesion values shown in Table II to those obtained from contact angle measurements, we consider four different cases which correspond to four different

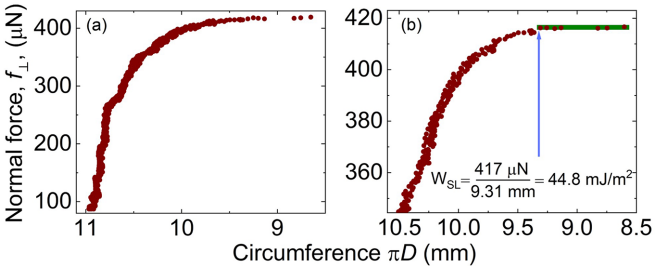

FIG. 5. (a) The circumference of the triple line of an 8.0-μl ethylene glycol drop on a PTFE surface vs the normal body force pulling on the drops. (b) Zoom-in on the end of the run presented in (a) where the blue arrow shows the values taken for the pull-off force and the pull-off diameter in Eq. (14). The green line corresponds to the green line in Fig. 1.

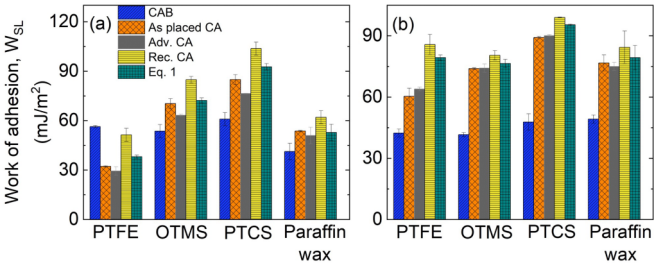

FIG. 6. Work of adhesion of water (a) and diiodomethane (b) with different solids based on: CAB measurements (blue) and contact angle measurements. CA stands for contact angle, Adv. stands for advancing, and Rec. stands for receding.

ways of measuring contact angles: (1) As-placed contact angle; (2) Advancing contact angle obtained by inflating the drop; (3) Receding contact angle obtained by deflating the drop; and (4) The calculated averaged equilibrium contact angle from the advancing receding contact angles [30]. In Fig. 6, W_{SL} represents the estimated work of adhesion for water with different solid surfaces using five different methods. Four of them are calculated from Eq. (12) for the four various ways of obtaining contact angles, and the fifth is the direct measurements of the work of adhesion obtained using CAB.

Two interesting features that Fig. 6 shows are the following:

(1) the work of adhesion values that are based on the visible contact angle measurements usually exceeds those based on CAB measurements, and

(2) The only exception to the observation above is the case of water on PTFE. This exception was found to be a reproducible trait of the PTFE-water system, while not being a trait of PTFE with any of the other liquids that we used. We explain this exception as follows: Surface adaptation results in two seemingly contradicting trends.

Trend 1: On one hand, surface adaptation causes the triple line to deform, which results in a macroscopic contact angle that is smaller than the nanoscopic one [16]. This results in an apparent W_{SL} that is higher than the true one; hence, apparently, $W_{SL,\ CAB} < W_{SL,\ CA}$.

Trend 2: On the other hand, the adaptation itself causes an increase in the solid-liquid work of adhesion (W_{SL}) as described below: If we consider the dry solid-vapor surface tension, $\gamma_{SV,dry}$, as a nonadapted surface, we can write, for the corresponding work of adhesion,

$$W_{SL,\ old} = \gamma_{SV,dry} + \gamma_{LV} - \gamma_{SL}, \tag{18}$$

where $W_{SL,\ old}$ represents the true work of adhesion for the case where the surface outside the drop is either dry or has never been adapted to a wet environment.

Yet, the CAB measured work of adhesion ($W_{SL,\ CAB}$) is done from a position at which outside the triple line there is a solid-vapor interface that has already been wetted by the liquid, and we mark this solid-vapor surface energy as $\gamma_{SV,\ wet}$. We can write

$$W_{SL,\ new} = \gamma_{SV,\ wet} + \gamma_{LV} - \gamma_{SL}. \tag{19}$$

Now, since $\gamma_{SV,\ wet} > \gamma_{SV,\ dry}$, we can write

$$W_{SL,\ new} - W_{SL,old} = \gamma_{SV,wet} - \gamma_{SV,dry} > 0. \tag{20}$$

Noting that the contact angle measurements are done when the solid-vapor interface is dry, we see that Eq. (20) can explain a situation in which CAB measurements give W_{SL} values that are higher than those measured through contact angles, for which the surface outside the drop is dry: $W_{SL,\ CAB} > W_{SL,\ CA}$.

It seems that unlike the other cases measured by us and by others [9,10,13,14], for the PTFE-water system trend 2 is more dominant.

According to this explanation, there should be a similarity between the work of adhesion measured by the CAB and

TABLE II. The work of adhesion measured using CAB ($W_{SL,\ CAB}$) for the different probe liquids on different solids, obtained from plots such as those shown in Figs. 4 and 5.

Probe liquids	PTFE (mJ/m^2)	OTMS (mJ/m^2)	PTCS (mJ/m^2)	Paraffin wax (mJ/m^2)
Water ($\gamma_{LV} = 72.8$ mN/m)	56.3 ± 0.7	53.6 ± 4.1	60.9 ± 4.3	41.3 ± 4.8
Glycerol ($\gamma_{LV} = 63.4$ mN/m)	49.2 ± 0.5	50.2 ± 2.2	56.9 ± 3.2	46.5 ± 3.3
Ethylene glycol ($\gamma_{LV} = 47.7$ mN/m)	43.8 ± 1.3	37.6 ± 2.1	45.2 ± 2.2	35.9 ± 3.9
Diiodomethane ($\gamma_{LV} = 50.8$ mN/m)	47.4 ± 1.2	41.6 ± 1.3	47.7 ± 3.3	49.2 ± 2.2

TABLE III. Corresponding x and y values in the linearized Eq. (15) for the given probe liquids on OTMS-coated silicon surface.

Probe liquids	$x = \sqrt{\frac{\gamma_{LV}^p}{\gamma_{LV}^d}}$	$y = \frac{W_{SL,\,CAB}}{2\sqrt{\gamma_{LV}^d}}$
Water	1.5	5.8 ± 0.45
Glycerol	0.94	4.3 ± 0.20
Ethylene glycol	0.81	3.5 ± 0.20
Diiodomethane	0.22	3.0 ± 0.10

that calculated using receding contact angles. Indeed, this similarity exists in our results.

In this context, we note that trend 1 is less significant for water than it is for diiodomethane for all substrates, with PTFE-water being the only case where it is smaller than trend 2. Trend 1 is also in agreement with the measurements done by several other groups [9–14], and in some cases [9,10] it is much more extreme than in our measurements, as described in the Appendix (see Fig. 12), and was attributed to the difference between the nanoscopic contact angle and the macroscopic one [16].

The energy difference associated with separating two surfaces is the work of adhesion. On the other hand, the energy difference associated with bringing them to contact can, in principle, be the same, but there are also suggestions that it may be greater, including attempts to relate it to contact angle hysteresis [53,54] for the case where the solid molecules do not undergo molecular reorientation. For the more general case that includes molecular reorientation, contact angle hysteresis mainly results from surface adaptation [16,17], which relates to lateral effects, not the normal work of adhesion. While it does not apply to the spontaneous shrinkage of the triple line, from which we obtain the work of adhesion, the hysteresis may relate to the path that leads to this event. Specifically, one can see in Figs. 4(b) and 5(b) that the initial part of the curve (before the blue arrow) follows an irregular shape. This irregularity may emanate from the same phenomena that lead to contact angle hysteresis as discussed above, but the point at which the spontaneous shrinkage of the triple line occurs is irrespective of that and is the same for different experiments. The fact that the critical value is the same regardless of the way the system reached that value is what one expects from a thermodynamic equilibrium.

Using Eq. (15) we can obtain four relations for the four probe liquids [see, e.g., Eqs. (A1) to (A4) and Table III in the Appendix]. For example, Fig. 7 shows the data points for the case of OTMS-coated silicon surface. The slope in Fig. 7 represents the polar component ($\sqrt{\gamma_{SV}^p}$), and the intercept with the y axis represents the dispersive component ($\sqrt{\gamma_{SV}^d}$) of the surface energy of the solid surface used.

From Fig. 7 we obtain the slope, $\sqrt{\gamma_{SV,\,OTMS}^p} = 1.3$, and the intercept with the y axis, $\sqrt{\gamma_{SV,\,OTMS}^d} = 2.8$, from which the surface energy of the OTMS-coated silicon surface is

$$\gamma_{SV,\,OTMS} = \gamma_{SV,\,OTMS}^d + \gamma_{SV,\,OTMS}^p = 9.9\,\frac{mJ}{m^2}. \quad (21)$$

Above, we demonstrated how to use CAB measurements to calculate solid-vapor surface energy. In Fig. 8, we compare it with the way such calculations are done with contact angles.

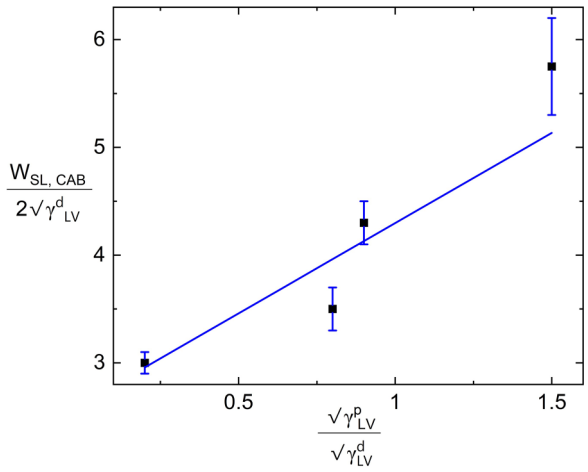

FIG. 7. A linear fit based on Eq. (15) for the calculation of γ_{SV}^p (the slope is $\sqrt{\gamma_{SV}^p}$, and γ_{SV}^d (the intercept is $\sqrt{\gamma_{SV}^d}$, for the OTMS-coated silicon surfaces based on the experimental data of the work of adhesion measured using CAB ($W_{SL,CAB}$).

Figures 8(a) and 8(b) present two important observations: (1) The curves that correspond to CAB measurements have a lower intercept with the y axis. This trend was consistent with all the surfaces that we measured. This represents a lower dispersive component of the surface energy of the solid; and (2) There seems to be a disagreement between the slopes corresponding to the contact angles, and between them and the slopes of the CAB measurements. Yet, there is actually some logic here too. For the paraffin wax, the slope corresponding to CAB measurements is significantly lower than the slopes corresponding to any of the contact angles. However, for OTMS the slope corresponding to CAB measurements is comparable to that of some of the contact angles (specifically, the advancing and the equilibrium contact angle). Noting that the slope represents the polar component of the surface energy, we shall see later on that this is also in agreement with other measurements where the CAB measurements show lower slopes for less-polar solid, and higher slopes for more-polar solid, while contact angles measurements lack a clear trend.

The surface-energy values based on plots such as those shown in Fig. 8 are calculated using Eq. (12) and presented

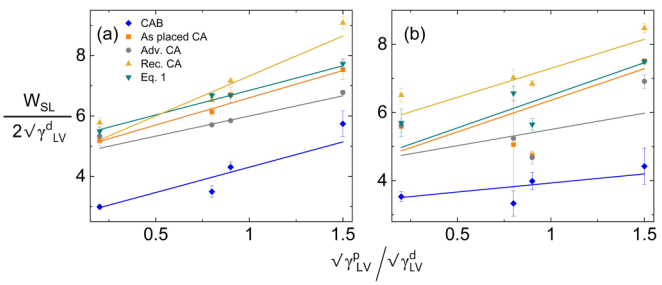

FIG. 8. Linear fits based on Eq. (15) for the calculation of γ_{SV}^p (the slope is $\sqrt{\gamma_{SV}^p}$, and γ_{SV}^d (the intercept is $\sqrt{\gamma_{SV}^d}$, for (a) OTMS-coated silicon surface and (b) paraffin wax surfaces, based on the experimental data of CAB (direct measurements of the work of adhesion, blue), and contact angle measurements.

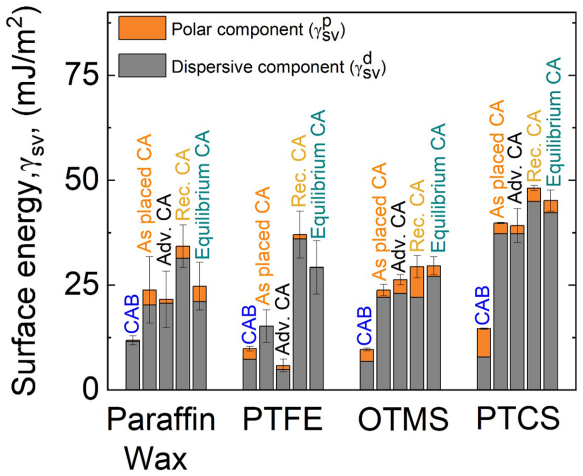

FIG. 9. Surface energy of different solids calculated using experimental data from CAB and contact angles.

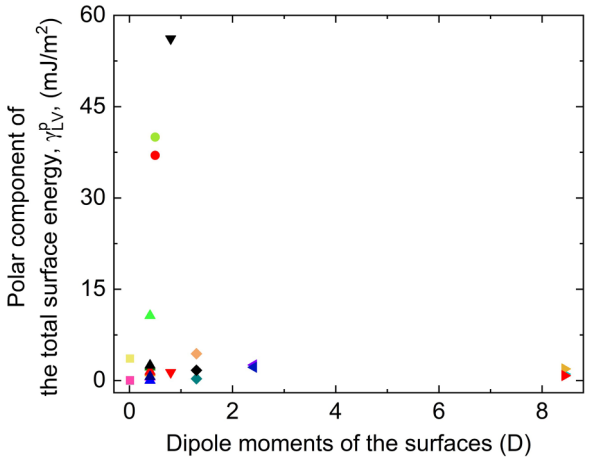

FIG. 11. Polar components of the surface energy for various surfaces based on other studies. Different surfaces are represented by distinct symbols and colors. Squares: paraffin wax [4,56–58]; triangles pointed up: PTFE [22,59–63]; circles: glass [64,65]; triangles pointing down: Polyethylene terephthalate (PET) [63,66]; diamonds: OTMS [67,68]; triangles pointing left: PTCS [69]; and triangles pointing right: Polydimethylsiloxane (PDMS) [63,70,71]. See the Appendix for more details.

in Fig. 9 for various solids. Several important features to note here include the following: those

(1) The solid surface energy obtained from work of adhesion measurements using the CAB is always lower than that obtained from contact angle measurements. Since lower work of adhesion values result in lower surface-energy values, then this is in agreement with other studies [9,10,13,55].

(2) The intercept with the y axis, which represents the dispersive component of the surface energy, is always lower for curves that correspond to CAB measurements than those that correspond to contact angle measurements. This is, again, in agreement with the studies mentioned above, and for the same reason (lower values of work of adhesion agree with lower values of surface energy).

(3) The slope of the curves, which represents the polar component of the surface energy, is sometimes lower and sometimes higher when corresponding to CAB measurements than when corresponding to contact angle measurements. This seems not to agree with the studies mentioned above for the cases in which the CAB-related values are higher. Yet, a closer look at those results shows that CAB-related values are higher for surfaces that are expected to be more polar. Thus, if comparing more-polar and less-polar solid surfaces, we see that surface-energy values obtained from CAB measurements are reasonable, while the ones from contact angle measurements are not.

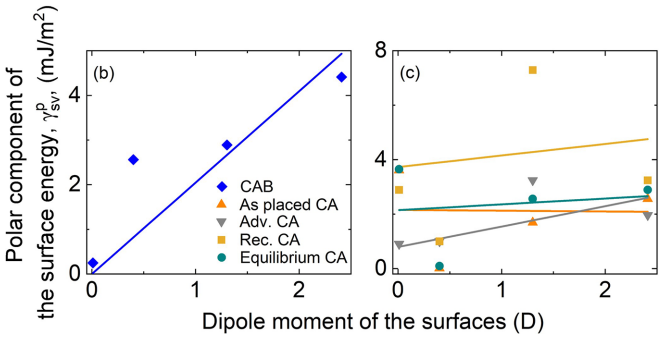

FIG. 10. Polar components of the surface energies for the four different surfaces plotted against their respective dipole moments, based on experimental data from (a) CAB and (b) contact angles.

To quantify this, Figs. 10(a) and 10(b) present the polar components of the surface energy (γ^p_{SV}) of the four solids versus their dipole moments. Figure 10(a) presents values obtained from CAB measurements and Fig. 10(b) presents values obtained from contact angle measurements. The order of surfaces presented in the x axis of Fig. 9 was made to match the increasing order of their dipole moments, starting from the lowest-dipole moment of paraffin wax and ending with the highest-dipole moment of PTCS. We see that the curve that corresponds to the CAB measurements intersects the origin of the axes as expected theoretically, while those corresponding to contact angle measurements do not. The slope of the curve is also reasonable for the CAB measurements, and less so for the contact angle measurements. Of the four different kinds of contact angles considered, the advancing contact angle gave the most reasonable trend, with the lowest y-axis interception and the highest slope.

In Fig. 11 we show the polar components of the surface energy of various surfaces, calculated from contact angle measurements reported in various other studies versus their respective dipole moments. We see that they do not follow a reasonable trend as lower-dipole moments correspond to higher-polar components of the surface energy. This supports our findings in Fig. 10(b), which shows that the contact angle measurements fail to reflect the relation between the polar components of the surface energy and the dipole moment of the corresponding surfaces. In contrast, CAB measurements show a reasonable correlation between the two.

V. CONCLUSION

The conventional approach to evaluate surface energy of solids is through breaking the surface energy to polar and

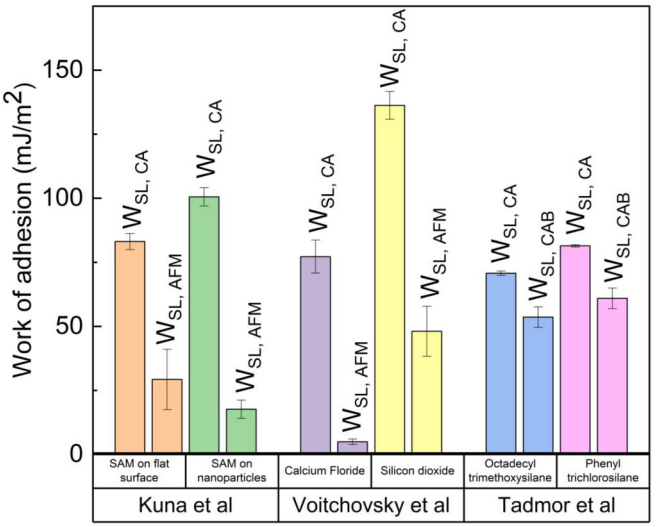

FIG. 12. Work of adhesion values of different solid-liquid pairs from independent experimental studies. Kuna *et al.* studied adhesion of water on self-assembled monolayer (SAM) and 3D SAM on nanoparticles. Voitchovsky *et al.* studied adhesion of water on calcium fluoride (CaF) and silicon oxide (SiO2) substrate. Tadmor *et al.* studied adhesion of water on OTMS and PTCS.

nonpolar components and using contact angle measurements to estimate the two components. Literature findings show that this method often leads to overestimation of the surface energy [9,10,13,55]. In this study, we introduce a method to evaluate the surface energy which is based on centrifugal adhesion balance (CAB) measurements. In agreement with the literature studies, CAB measurements also result in surface-energy values that are significantly lower than those obtained through contact angle measurements.

In addition, to quantify how reasonable the surface-energy evaluations based on CAB measurements are, we use the fact that materials with higher-dipole moment are also more polar; hence, there needs to be a correlation between the polar component of the surface energy and the dipole moment. Our paper shows that the contact angle measurements do not result in a reasonable correlation between the polar components of

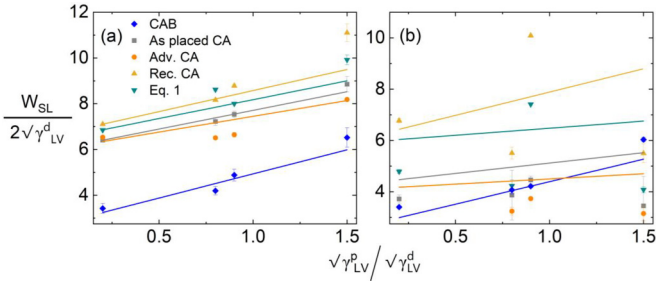

FIG. 13. Linear fits based on Eq. (15) for the calculation of γ_{SV}^{p} (the slope is $\sqrt{\gamma_{SV}^{p}}$, and γ_{SV}^{d} (the intercept is $\sqrt{\gamma_{SV}^{d}}$, for (a) PTCS-coated silicon surface and (b) PTFE surface, based on the experimental data of CAB (direct measurements of the work of adhesion, brown), as-placed contact angle (black), advancing contact angle (red), receding contact angle (blue), and equilibrium contact angle (green).

TABLE IV. The P_{LL}, R_{LL}, and μ values calculated for paraffin wax and PTFE.

Surface	P_{LL}	R_{LL}	$\mu = \sqrt{\frac{P_{LL}-R_{LL}}{20.6}}$ (D)
Paraffin wax	4.65	4.649	0.007
PTFE	12.36	8.752	0.4

the surface energy and the dipole moments of the surfaces. On the other hand, CAB measurements provide a good correlation between the two.

ACKNOWLEDGMENTS

This study was supported by a grant from the Israeli Ministry of Science and Technology. We also acknowledge support from Hy Greenhill Chair in Theoretical and Applied Mechanics and from the Pearlstone Center.

APPENDIX

Figure 12 shows a comparison between work of adhesion measured by Kuna *et al.* [9], Voitchovsky *et al.* [10], and Tadmor *et al.* [14] to the work of adhesion calculated using the Young-Dupre equation based on contact angle measurements.

TABLE V. Details regarding the distinct symbols and colors used to represent the surfaces in Fig. 11, and the references used.

Surface: legend symbol	Legend symbol's color	References
Paraffin wax (Square)	Black	
	Yellow	This paper
	Red	
	Blue	
	Pink	
OTMS (Triangle pointing up)	Green	
	Orange	
	Cyan	
	Red	
	Pink	
	Blue	
	Black	
	Altay	
	Dark blue	This paper
PTFE (Circles)	Red	
	Green	
Glass (Triangle pointing down)	Black	
	Red	
PET (Diamonds)	Green	
	Yellow	
	Black	This paper
PTCS (Triangle pointing left)	Blue	This paper
	Black	
PDMS (Triangle pointing right)	Green	
	Yellow	
	Owen	

1. Sample calculation for OTMS-coated silicon surface

Using Eq. (15) and the values presented in Table I for γ_{LV}^{p} and γ_{LV}^{d}, we write the corresponding relations for each of the probe liquids in Eqs. (A1) to (A4):

$$\text{Water}: \quad \frac{W_{SL}}{2\sqrt{21.8}} = \sqrt{\gamma_{SV}^{d}} + \sqrt{\gamma_{SV}^{p}}\left(\sqrt{\frac{51.0}{21.8}}\right), \tag{A1}$$

$$\text{Glycerol}: \quad \frac{W_{SL}}{2\sqrt{37.0}} = \sqrt{\gamma_{SV}^{d}} + \sqrt{\gamma_{SV}^{p}}\left(\sqrt{\frac{30.0}{37.0}}\right), \tag{A2}$$

$$\text{Ethylene glycol}: \quad \frac{W_{SL}}{2\sqrt{29.0}} = \sqrt{\gamma_{SV}^{d}} + \sqrt{\gamma_{SV}^{p}}\left(\sqrt{\frac{19.0}{29.0}}\right), \tag{A3}$$

$$\text{Diiodomethane}: \quad \frac{W_{SL}}{2\sqrt{48.5}} = \sqrt{\gamma_{SV}^{d}} + \sqrt{\gamma_{SV}^{p}}\left(\sqrt{\frac{2.3}{48.5}}\right). \tag{A4}$$

In Table III we list the values obtained from our measurements with the probe liquids on OTMS-coated silicon surfaces.

The values in Table III are used for the curve in Fig. 7. The slope from Fig. 7 represents the polar component ($\sqrt{\gamma_{SV}^{p}}$), and the y intercept represents the dispersive component ($\sqrt{\gamma_{SV}^{d}}$) of the surface energy of the solid surface used.

2. Graphs that are used to calculate the surface energies of PTCS-coated silicon and PTFE surfaces

Figure 13 shows a graphical representation of the slopes and y axis intercepts based on Eq. (15) for two different surfaces, considering four different methods.

3. Calculation of the dipole moments (μ) of the four surfaces

The dielectric moments of polymers are found out using Debye's equation [72] [given below as Eq. (A5)]:

$$P_{LL} - R_{LL} = 20.6\,\mu^2, \tag{A5}$$

where P_{LL} is the molar dielectric polarization according to Lorentz and Lorenz, R_{LL} is the molar refraction according to Lorentz and Lorenz, and μ is the dipole moment of the polymer.

Table IV below shows the corresponding P_{LL}, R_{LL}, and μ calculated for each polymer.

The dipole moments of OTMS and PTCS were obtained from Yaw's critical property data for chemical engineers and chemists [73].

4. Details of references regarding Fig. 11

Table V below shows the details regarding the references used for Fig. 11.

[1] A. Marmur, Soft contact: Measurement and interpretation of contact angles, Soft Matter **2**, 12 (2006).

[2] W. A. Zisman, Relation of the equilibrium contact angle to liquid and solid constitution, Adv. Chem. **43**, 1 (1964).

[3] W. A. Zisman, Influence of constitution on adhesion, Ind. Eng. Chem. **55**, 18 (1963).

[4] D. K. Owens and R. C. Wendt, Estimation of the surface free energy of polymers, J. Appl. Polym. Sci. **13**, 1741 (1969).

[5] C. A. Ward and A. W. Neumann, On the surface thermodynamics of a two-component liquid-vapor-ideal solid system, J. Colloid Interface Sci. **49**, 286 (1974).

[6] C. J. V. Oss, R. J. Good, and H. J. Busscher, Estimation of the polar surface tension parameters of glycerol and formamide, for use in contact angle measurements on polar solids, J. Dispers. Sci. Technol. **11**, 75 (1990).

[7] J. C. Berg, The importance of acid-base interactions in wetting, coating, adhesion and related phenomena, Nord Pulp Paper Res. J. **8**, 75 (1993).

[8] N. T. Correia, J. J. M. Ramos, B. J. V. Saramago, and J. C. G. Calado, Estimation of the surface tension of a solid: Application to a liquid crystalline polymer, J. Colloid Interface Sci. **189**, 361 (1997).

[9] J. J. Kuna, K. Voïtchovsky, C. Singh, H. Jiang, S. Mwenifumbo, P. K. Ghorai, M. M. Stevens, S. C. Glotzer, and F. Stellacci, The effect of nanometre-scale structure on interfacial energy, Nat. Mater. **8**, 837 (2009).

[10] K. Voïtchovsky, J. J. Kuna, S. A. Contera, E. Tosatti, and F. Stellacci, Direct mapping of the solid-liquid adhesion energy with subnanometre resolution, Nat. Nanotechnol. **5**, 401 (2010).

[11] W. Park, S. Müller, R. P. Baumann, S. Becker, and B. Hwang, Surface energy characterization of nanoscale metal using quantitative nanomechanical characterization of atomic force microscopy, Appl. Surf. Sci. **507**, 145041 (2020).

[12] B. Sauerer, M. Stukan, W. Abdallah, M. H. Derkani, M. Fedorov, J. Buiting, and Z. J. Zhang, Quantifying mineral surface energy by scanning force microscopy, J. Colloid Interface Sci. **472**, 237 (2016).

[13] A. P. Defante, T. N. Burai, M. L. Becker, and A. Dhinojwala, Consequences of water between two hydrophobic surfaces on adhesion and wetting, Langmuir **31**, 2398 (2015).

[14] R. Tadmor, R. Das, S. Gulec, J. Liu, H. E. N'guessan, M. Shah, P. S. Wasnik, and S. B. Yadav, Solid-liquid work of adhesion, Langmuir **33**, 3594 (2017).

[15] M. S. Sadullah, Y. Xu, S. Arunachalam, and H. Mishra, Predicting droplet detachment force: Young-Dupré model fails, Young-Laplace model prevails, Commun. Phys. **7**, 89 (2024).

[16] R. Tadmor, Open problems in wetting phenomena: Pinning retention forces, Langmuir **37**, 6357 (2021).

[17] H. J. Butt, R. Berger, W. Steffen, D. Vollmer, and S. A. L. Weber, Adaptive wetting-adaptation in wetting, Langmuir **34**, 11292 (2018).

[18] L. Chen, E. Bonaccurso, T. Gambaryan-Roisman, V. Starov, N. Koursari, and Y. Zhao, Static and dynamic wetting of soft substrates, Curr. Opin. Colloid Interface Sci. **36**, 46 (2018).
[19] G. R. Lester, Contact angles of liquids on organic solids, Nature (London). **209**, 1126 (1966).
[20] A. Carré, J. C. Gastel, and M. E. R. Shanahan, Viscoelastic effects in the spreading of liquids, Nature (London) **379**, 432 (1996).
[21] E. Bormashenko and Y. Bormashenko, Wetting of composite surfaces: When and why is the area far from the triple line important?, J. Phys. Chem. C **117**, 19552 (2013).
[22] Z. Chen and M. Nosonovsky, Revisiting lowest possible surface energy of a solid, Surf Topogr. **5**, 045001 (2017).
[23] D. Y. Kwok, H. Ng, and A. W. Neumann, Experimental study on contact angle patterns: Liquid surface tensions less than solid surface tensions, J. Colloid Interface Sci. **225**, 323 (2000).
[24] R. R. Deshmukh and A. R. Shetty, Comparison of surface energies using various approaches and their suitability, J. Appl. Polym. Sci. **107**, 3707 (2008).
[25] R. Tadmor and P. S. Yadav, As-placed contact angles for sessile drops, J. Colloid Interface Sci. **317**, 241 (2008).
[26] E. Bormashenko, Progress in understanding wetting transitions on rough surfaces, Adv. Colloid Interface Sci. **222**, 92 (2015).
[27] F. Chen, Y. Wang, Y. Tian, D. Zhang, J. Song, C. R. Crick, C. J. Carmalt, I. P. Parkin, and Y. Lu, Robust and durable liquid-repellent surfaces, Chem. Soc. Rev. **51**, 8476 (2022).
[28] C. W. Extrand, Comment on "Solid-Liquid Work of Adhesion," Langmuir **33**, 36 (2017).
[29] S. Gulec, S. Yadav, R. Das, and R. Tadmor, Reply to Comment on "Solid-Liquid Work of Adhesion," Langmuir **33**, 13899 (2017).
[30] R. Tadmor, Line energy and the relation between advancing, receding, and Young contact angles, Langmuir **20**, 7659 (2004).
[31] K. Terpiłowski, A. E. Wiącek, and M. Jurak, Influence of nitrogen plasma treatment on the wettability of polyetheretherketone and deposited chitosan layers, Adv. Polym. Technol. **37**, 1557 (2018).
[32] S. Parvate, P. Dixit, and S. Chattopadhyay, Superhydrophobic surfaces: Insights from theory and experiment, J. Phys. Chem. B **124**, 1323 (2020).
[33] M. Azadi Tabar, M. H. Ghazanfari, and A. Dehghan Monfared, On the size-dependent behavior of drop contact angle in wettability alteration of reservoir rocks to preferentially gas wetting using nanofluid, J. Pet. Sci. Eng. **178**, 1143 (2019).
[34] M. Hernaiz *et al.*, The contact angle of nanofluids as thermophysical property, J. Colloid Interface Sci. **547**, 393 (2019).
[35] A. Vinod, Y. V. Reddy Bhimavarapu, M. Hananovitz, Y. Stern, S. Gulec, A. K. Jena, S. Yadav, E. J. Gutmark, P. K. Patra, and R. Tadmor, Mucus-inspired tribology, a sticky yet flowing hydrogel, ACS Appl. Polym. Mater. **4**, 8527 (2022).
[36] S. Gulec, S. Yadav, R. Das, V. Bhave, and R. Tadmor, The influence of gravity on contact angle and circumference of sessile and pendant drops has a crucial historic aspect, Langmuir **35**, 5435 (2019).
[37] J. W. Drelich, Contact angles: From past mistakes to new developments through liquid-solid adhesion measurements, Adv. Colloid Interface Sci. **267**, 1 (2019).
[38] P. Sundriyal, M. Pandey, and S. Bhattacharya, Plasma-assisted surface alteration of industrial polymers for improved adhesive bonding, Int. J. Adhes. Adhes. **101**, 102626 (2020).
[39] F. M. Fowkes, Attractive forces at interfaces, Ind. Eng. Chem. **56**, 40 (1964).
[40] J. Wei and Y. Zhang, Application of sessile drop method to determine surface free energy of asphalt and aggregate, J. Test. Eval. **40**, 807 (2012).
[41] D. H. Kaelble, Dispersion-polar surface tension properties of organic solids, J. Adhes. **2**, 66 (1970).
[42] D. Y. Kwok and A. W. Neumann, Contact angle measurement and contact angle interpretation, Adv. Colloid Interface Sci. **81**, 167 (1999).
[43] E. N. Dalai, Calculation of solid surface tensions, Langmuir **3**, 1009 (1987).
[44] A. Carré, Polar interactions at liquid/polymer interfaces, J. Adhes. Sci. Technol. **21**, 961 (2007).
[45] A. Kozbial, Z. Li, C. Conaway, R. McGinley, S. Dhingra, V. Vahdat, F. Zhou, B. Durso, H. Liu, and L. Li, Study on the surface energy of graphene by contact angle measurements, Langmuir **30**, 8598 (2014).
[46] P. S. Wasnik, H. E. N'guessan, and R. Tadmor, Controlling arbitrary humidity without convection, J. Colloid Interface Sci. **455**, 212 (2015).
[47] D. W. Pilat, P. Papadopoulos, D. Schäffel, D. Vollmer, R. Berger, and H. J. Butt, Dynamic measurement of the force required to move a liquid drop on a solid surface, Langmuir **28**, 16812 (2012).
[48] M. Beitollahpoor, M. Farzam, and N. S. Pesika, Friction force-based measurements for simultaneous determination of the wetting properties and stability of superhydrophobic surfaces, J. Colloid Interface Sci. **648**, 161 (2023).
[49] N. Gao, F. Geyer, D. W. Pilat, S. Wooh, D. Vollmer, H. J. Butt, and R. Berger, How drops start sliding over solid surfaces, Nat. Phys. **14**, 191 (2018).
[50] D. Patel, Y. V. Reddy Bhimavarapu, A. K. Jena, R. Tadmor, and T. Cai, Non-invasive rust detection of steel plates determined through interfacial modulus, Front. Chem. Eng. **5**, 1150776 (2023).
[51] A. Vinod, R. Tadmor, D. Katoshevski, and E. J. Gutmark, Gels that serve as mucus simulants: A review, Gels **9**, 555 (2023).
[52] S. Tang, Y. Bhimavarapu, S. Gulec, R. Das, J. Liu, H. N'Guessan, T. Whitehead, C. W. Yao, and R. Tadmor, Droplets sliding down a vertical surface under increasing horizontal forces, Langmuir **35**, 8191 (2019).
[53] M. Nosonovsky, Model for solid-liquid and solid-solid friction of rough surfaces with adhesion hysteresis, J. Chem. Phys. **126**, 224701 (2007).
[54] M. Nosonovsky and R. Ramachandran, Geometric interpretation of surface tension equilibrium in superhydrophobic systems, Entropy **17**, 4684 (2015).
[55] A. Narayanan, A. Dhinojwala, and A. Joy, Design principles for creating synthetic underwater adhesives, Chem. Soc. Rev. **50**, 13321 (2021).
[56] B. Jańczuk and T. Białłopiotrowicz, Surface free-energy components of liquids and low energy solids and contact angles, J. Colloid Interface Sci. **127**, 189 (1989).
[57] A. El-shimi and E. D. Goddard, Wettability of some low energy surfaces. I. Air/liquid/solid interface, J. Colloid Interface Sci. **48**, 242 (1974).
[58] J. R. Dann, Forces involved in the adhesive process. I. Critical

surface tensions of polymeric solids as determined with polar liquids, J. Colloid Interface Sci. **32**, 302 (1970).

[59] H. W. Fox and W. A. Zisman, The spreading of liquids on low-energy surfaces. II. Modified tetrafluoroethylene polymers, J. Colloid Sci. **7**, 109 (1952).

[60] H. Kobayashi and M. J. Owen, Surface tension of poly [(3,3,4,4,5,5,6,6,6-nonafluorohexyl)-methylsiloxane], Macromolecules **23**, 4929 (1990).

[61] N. Selvakumar, H. C. Barshilia, and K. S. Rajam, Effect of substrate roughness on the apparent surface free energy of sputter deposited superhydrophobic polytetrafluoroethylene coatings: A comparison of experimental data with different theoretical models, J. Appl. Phys. **108**, 013505 (2010).

[62] D. Wang and C. J. Cornelius, Ionomer thermodynamic interrelationships associated with wettability, surface energy, swelling, and water transport, Eur. Polym. J. **85**, 126 (2016).

[63] B. N. Altay *et al.*, Surface free energy estimation: A new methodology for solid surfaces, Adv. Mater. Interfaces **7**, 1901570 (2020).

[64] C. M. Gatley-Montross *et al.*, Multivariate analysis of attachment of biofouling organisms in response to material surface characteristics, Biointerphases **12**, 051003 (2017).

[65] G. Soliveri, R. Annunziata, S. Ardizzone, G. Cappelletti, and D. Meroni, Multiscale rough titania films with patterned hydrophobic/oleophobic features, J. Phys. Chem. C **116**, 26405 (2012).

[66] K. Song, J. Lee, S.-O. Choi, and J. Kim, Interaction of surface energy components between solid and liquid on wettability, and its application to textile anti-wetting finish, Polymers (Basel) **11**, 498 (2019).

[67] G. Lamour, A. Eftekhari-Bafrooei, E. Borguet, S. Souès, and A. Hamraoui, Neuronal adhesion and differentiation driven by nanoscale surface free-energy gradients, Biomaterials **31**, 3762 (2010).

[68] B. King, C. L. Radford, M. C. Vebber, B. Ronnasi, and B. H. Lessard, Not just surface energy: The role of bis(pentafluorophenoxy) silicon phthalocyanine axial functionalization and molecular orientation on organic thin-film transistor performance, ACS Appl. Mater. Interfaces **15**, 14937 (2022).

[69] P. Pacher *et al.*, Characterizing chemically reactive thin layers: Surface reaction of [2-[4-(Chlorosulfonyl)Phenyl]Ethyl]Trichlorosilane with ammonia, J. Phys. Chem. C **111**, 12407 (2007).

[70] M. J. Owen, Surface tension of Polytrifluoropropylmethylsiloxane, J. Appl. Polym. Sci. **35**, 895 (1988).

[71] Z. Zhang, Polar and dispersive surface tension components of water-guanidinium chloride (Gdmcl) binary mixtures, Colloids Surf. A: Physicochem. Eng. Asp. **676**, 132223 (2023).

[72] D. W. Van Krevelen, *Properties of Polymers: Their Correlation with Chemical Structure; Their Numerical Estimation and Prediction from Additive Group Contributions*, 3rd ed. (Elsevier, 1990), p. 87.

[73] C. L. Yaws, *Yaws' Critical Property Data for Chemical Engineers and Chemists* (Knovel, 2012).